RESEARCH ARTICLE
SPACE PHYSICS: IONOSPHERIC PHYSICS

Earth and Planetary Physics
8: 742–752, 2024
doi: 10.26464/epp2024037

Long-term variation of Arctic Sudden Stratospheric Warmings (SSW) and potential causes

QingRan Li[1], ShaoDong Zhang[1,2,3,4*], KaiMing Huang[1,3], ChunMing Huang[1,3], Yun Gong[1,3], WenTao Tang[5], and Zheng Ma[1,3]

[1]School of Electronic Information, Wuhan University, Wuhan 430072, China;

[2]Guizhou Normal University, Guiyang 550001, China;

[3]Key Laboratory of Geospace Environment and Geodesy, Ministry of Education, Wuhan 430072, China;

[4]State Key Laboratory of Information Engineering in Surveying, Mapping and Remote Sensing, Wuhan 430072, China;

[5]School of Electronic Information Engineering, Jingchu University of Technology, Jingmen 448000, China

Key Points:

- We find that weakening polar vortices and enhancing planetary waves caused increases in Sudden Stratospheric Warming (SSW) events over the 41 winters (1979/1980–2019/2020), and vice versa.
- Within an overall increase in SSW events during this period, SSW duration and strength tended to increase from 1979 to 2001 and then began to decrease from 2001 to 2020.
- The variation of Planetary Wave 1 (PW1) appears to be the main contributor to long-term trends of planetary waves as well as SSWs.

Citation: Li, Q. R., Zhang, S. D., Huang, K. M., Huang, C. M., Gong, Y., Tang, W. T., and Ma, Z. (2024). Long-term variation of Arctic Sudden Stratospheric Warmings (SSW) and potential causes. *Earth Planet. Phys.*, *8*(5), 742–752. http://doi.org/10.26464/epp2024037

Abstract: Utilizing the European Centre for Medium-Range Weather Forecast (ECMWF) Reanalysis v5 (ERA5), for the first time, we have confirmed close links among Sudden Stratospheric Warmings (SSWs) in the Northern Hemisphere (NH), the polar vortices, and stratospheric Planetary Waves (PWs) by analyzing and comparing their trends. Interestingly, within overall increasing trends, the duration and strength of SSWs exhibit increasing and decreasing trends before and after the winter of 2002, respectively. To reveal possible physical mechanisms driving these trends, we analyzed the long-term trends of the winter (from December to February) polar vortices and of stratospheric PWs with zonal wave number 1. Notably, our results show that in all three time periods (the entire period of 41 winters, 1980 to 2020, and the two subperiods — 1980–2002 and 2002–2020) enhancing SSWs were always accompanied by weakening winter polar vortices and strengthening polar PWs like Stationary Planetary Waves (SPWs) and 16-day waves, and vice versa. This is the first proof, based on ERA5 long-term trend data, that weakening polar vortices and enhancing stratospheric PWs (especially SPWs) could cause an increase in SSWs.

Keywords: sudden stratospheric warmings; stationary planetary waves; 16-day waves; polar vortrices; long-term trend; correlation coefficient

1. Introduction

As the most dramatic stratospheric phenomenon, Sudden Stratospheric Warmings (SSWs) occur during extended winter, and almost exclusively in the Northern Hemisphere (NH). When an SSW happens, it is accompanied by polar warming of up to 50°C over a week or two, and the normally strong wintertime westerly stratospheric circulation breaks down in a few days, replaced by weak easterly winds (Baldwin et al., 2021). SSWs occurring in the polar stratosphere can affect the extratropical troposphere and mesosphere, such as the tropospheric jet stream, storm tracks, and precipitation (O'Neill et al., 2015), and high-latitude cooling in the mesosphere, along with a reversal of the zonal mean zonal winds from easterly to westerly (the opposite as in the stratosphere) (Walterscheid et al., 2000). In addition to the extratropical region, many studies have also revealed intensive impacts of SSWs on planetary and tidal waves in the mesosphere and ionosphere above the mid-latitudes (Ma Z et al., 2017). Changes in stratospheric mesospheric chemistry and zonal winds during an SSW affect solar and lunar atmospheric tides, which in turn play a key role in the coupling of SSWs with mesosphere and ionosphere variability (Goncharenko et al., 2012; Chau et al., 2015). The physics of SSWs also results in the dissipation of enhanced semidiurnal and lunar tides leading to global latitudinal cooling, which significantly alters the circulation in the lower thermosphere (Liu HX et al., 2014). Increasing observations have revealed strong disturbances below and above the stratosphere in the low-lati-

First author: Q. R. Li, liqingran@whu.edu.cn
Correspondence to: S. D. Zhang, zsd@whu.edu.cn
Received 15 JAN 2024; Accepted 19 MAY 2024.
First Published online 15 JUL 2024.

tudes and mid-latitudes (Pedatella et al., 2016). Moreover, recent studies have suggested that SSWs could also lead to inter-hemisphere responses (Yamazaki et al., 2020).

The important influences of SSWs on the global atmosphere have led many researchers to investigate possible trigger mechanisms (Polvani and Waugh, 2004; Scott and Polvani, 2006). The most widely accepted theory is the wave-mean flow interaction (Matsuno, 1971). When Planetary Waves (PWs) propagate upward from the troposphere into the stratosphere, they can deposit heat and momentum into the stratospheric atmosphere, then raise the temperature and reduce the wind field (a minor SSW), or even cause a stratospheric wind field reversal (a major SSW). This dramatic dynamical process can influence the polar and equatorial meridional circulation and thus change the transportation of constituents, such as ozone and other trace gases, then exert impacts on atmospheric chemistry throughout the lower and middle stratosphere (e.g., Baldwin and Holton, 1988; Manney et al., 2009a; de la Cámara et al., 2018). SSWs could also enhance eastward gravity wave forcing and migrating of solar and lunar semidiurnal tides, and could alter chemistry and dynamics in the mesosphere, ionosphere, and thermosphere (Gong Y et al., 2018; Li YX et al., 2021; Ning WH et al., 2022; Zeng XY and Zhong G, 2024). Therefore, SSWs can affect the global atmosphere above the troposphere.

It is now widely accepted that planetary wave propagation and breaking play a key role in the triggering and evolution of SSWs (Baldwin and Holton, 1988). Most SSWs are accompanied by dramatic variations in PWs (Limpasuvan et al., 2004; Pogoreltsev et al., 2015). Among different PW modes, quasi-stationary waves and 16-Day Waves (16DWs) are believed to be the most important contributors to SSWs (Gong Y et al., 2019; Li W et al., 2021). The effect of quasi-stationary waves in the stratosphere is to warm the pole and decelerate the polar jet (Lin BD, 1982). As a significant large-scale wave in the stratosphere, the traveling 16DW from the troposphere can warm the polar stratosphere (Pancheva et al., 2008; Coy et al., 2009). Moreover, different wave numbers of the quasi-stationary waves and 16DWs determine the different types of SSWs (Charlton and Polvani, 2007). Waves with zonal wavenumbers 1 and 2 are observed generally to displace the polar vortices poleward (Castanheira and Barriopedro, 2010) and split the polar vortices (Martius et al., 2009), respectively. The other important element in the triggering of SSWs is the polar vortex (Ma Z et al., 2020). SSWs are usually a consequence of polar vortex breakdown in the stratosphere (Matthewman et al., 2009); a typical polar vortex is deemed to hinder the propagation of tropospheric PWs into the stratosphere, thus impeding the onset of SSWs (Ambaum and Hoskins, 2002; Solomon, 2014).

Most previous research (Manney et al., 2009b; Tao M et al., 2015) on SSWs and their links to polar vortices and PWs has been based on case studies; relatively few investigations have focused on long-term patterns of change. Even fewer studies have compared long-term trends of SSWs, polar vortices, and PWs. Therefore, although case studies have improved our understanding of long-term trends in SSWs, polar vortices, and PWs, links among these phenomena and causes of the long-term variations of SSWs remain unclear. It is well accepted that the main SSW trigger mechanism is probably an interaction of polar vortices and upward propagating PWs. Therefore, the main purpose of this study is to investigate long-term trends in SSWs and analyze correlations between these trends and long-term variations of polar vortices and PWs. The remainder of this manuscript is organized as follows. In Section 2, below, we introduce our data processing methods. In Section 3, Results, we present long-term trends of the SSWs, long-term trends of the polar vortices, and long-term trends of planetary waves. All three subsections present data from a specific period and note different trends in that period. In the last section, we provide a summary of our analyses.

2. Data and Methods

In this paper, temperature and zonal wind data are utilized to investigate stratospheric SSWs and PWs, depending on the definition of SSW, the method of extracting perturbations, and the process of fitting temperature/wind amplitudes; polar vortices are investigated based on monthly averaged *Potential Vorticity* (PV) data; like previous studies, we use PV data to represent the polar vortex (Manney et al., 2011; Lawrence et al., 2015; Zhang MH et al., 2019). Therefore, all the calculations about the polar vortices in this paper are based on PV data and we use Potential *Vorticity* Anomaly (PVA) data to represent the polar *vortex* anomaly (the strength of the polar vortex). We use temperature, PV, and horizontal winds data from the European Centre for Medium-Range Weather Forecast (ECMWF) Reanalysis v5 (ERA5), a state-of-the-art global atmospheric reanalysis (Hersbach et al., 2020), produced by the Copernicus Climate Change Service (C3S). The dataset is archived on a global grid with high spatial resolution (0.25° longitude × 0.25° latitude) and 37 pressure levels (1000 hPa correlation coefficient hPa), currently available from January 1940 to the present. The vertical resolution of the data varies from several hundreds of meters in the troposphere to ~5 km at the stratopause. To compare our results quantitatively with previous work by Li Y et al. (2023), Li YP and Wen ZP (2021, 2022), Hu DZ et al. (2019), Tang WT et al. (2021), etc., which were based on data from the Modern-Era Retrospective Analysis for Research and Applications version 2 (MERRA2), we limit this study to ERA5 NH reanalysis data from December 1979 to February 2020, matching the same time period and geographic region they studied.

We calculate daily averages of the original 6-hourly data to identify SSWs. An SSW event is identified based on the World Meteorological Organization (WMO) definition: the zonal mean temperature gradient between 90°N and 60°N becomes positive, and the positive gradient lasts more than 5 days at 10 hPa levels. There are two types of SSWs — a major SSW, accompanied by a (zonally-averaged) wind reversal at 60°N at 10 hPa; a minor SSW, for which there is only a temperature gradient inversion but no zonal wind inversion at 10 hPa. The Final Stratospheric Warming (FSW) each year is the warming accompanied by zonal wind speed gradient reversal that does not again reverse. SSWs usually occur in the NH winter, while FSWs occur from March to May. Our paper focuses mainly on SSWs and how they are related to polar vortices and planetary waves. Therefore, two additional criteria are employed here to avoid overestimating the number of midwinter SSWs. First, to avoid double counting, we check if a previous SSW has been recorded in the 5 immediately preceding days; if so, an interval of 20 consecutive days with westerly winds must exist before the following central date can be defined (Charlton and Polvani, 2007). Second, to ensure that no FSW (the earliest occur in March) is counted, this study includes no events detected after the end of February, a criterion that differs from Charlton and Polvani (2007).

In our study, we choose two parameters to describe the characteristics of SSWs. One is their duration — the number of days when the temperature gradient between 60°N and 90°N at 10 hPa becomes reversed. The other is the SSW's strength — defined as the maximum daily mean temperature gradient between latitudes 60°N and 90°N at 10 hPa. More detailed definitions of the duration and strength of SSWs are referred to Li YP et al. (2018). For example, as shown in Figure 1, which portrays the 2018-19 SSW, the stratospheric temperature began to warm in December 2018, the zonal mean temperature at 90°N reaching its maximum on December 28. Thus, according to the above SSW duration (defined by the meridional temperature gradient at 10 hPa), only one SSW event — confined to December and January — occurred in the winter of 2018–2019. The onset day was December 25, 2018, and the date of decay was January 16, 2019, so the duration of the single SSW in that year was 23 days. The maximum daily temperature difference (outbreak day) occurred on December 28, 2018: the temperature at 10 hPa height was 260.0 K at 90°N; it was 226.2 K at 60°N, a difference of 33.8 K. So, by the strength definition, the strength of the sole SSW in the winter of 2018–2019 was 33.8 K. The SSW's wind field reversed on January 3 and remained reversed until January 16.

As we know, the interaction of polar vortices and upward propagating planetary waves is proposed to be the main trigger mechanism for SSW; and SSWs are usually thought to be a consequence of polar vortex breakdown. Thus, we will study long-term trends in polar vortices and PWs in the following context. Since PV is conserved and advected along isentropic surfaces, in the absence of diabatic heating and friction, we use polar PV-based measurements between 60°N and 90°N to diagnose the intensities of the polar vortices (Nash et al., 1996). The Potential Vorticity Unit (PVU,1 PVU = 10^{-6} K · m^2 · s^{-1} · kg^{-1}) is used to define PV intensities. We take the monthly and zonal mean PV intensities, averaged over 60°N and 90°N, from ERA5 as characterizing the polar vortex in the NH. The composite annual variation in the polar vortex, in each of the three winter months, averaged over 41 winters, is taken as the monthly mean polar vortex. Then, the polar vortex anomaly, i.e., PV′ (PVA for a specific winter month), is calculated by subtracting the 41-year monthly mean PV in the same month from that year's polar vortex. Then, for each year, we calculate the mean PV′ in the three winter months as the annual mean polar vortex anomaly.

The other important element in the triggering of SSWs is the planetary wave. Among different planetary wave modes (Matthias et al., 2012; Sassi et al., 2012; Huang CM et al., 2021; Ma Z et al., 2024), Stationary Planetary Waves (SPWs) and 16DWs are considered to be the most closely related to SSW events (Vineeth et al., 2009; Limpasuvan et al., 2016; Gong Y et al., 2019). Temperature perturbations of SPWs are extracted by the following steps: (1) A zonally averaged temperature is removed, as the background component, from the monthly averaged temperature; then the residual components can be thought to be the stationary wave components with different zonal wavenumbers; (2) For specific height and latitude, the height and latitude dependent wave amplitudes of stationary waves with wavenumbers 1 and 2 are determined by a harmonic fitting on the residual components, according to Equation (1) (Wu DL et al., 1995):

$$T'(\lambda) = A\cos(s\lambda + \varphi), \tag{1}$$

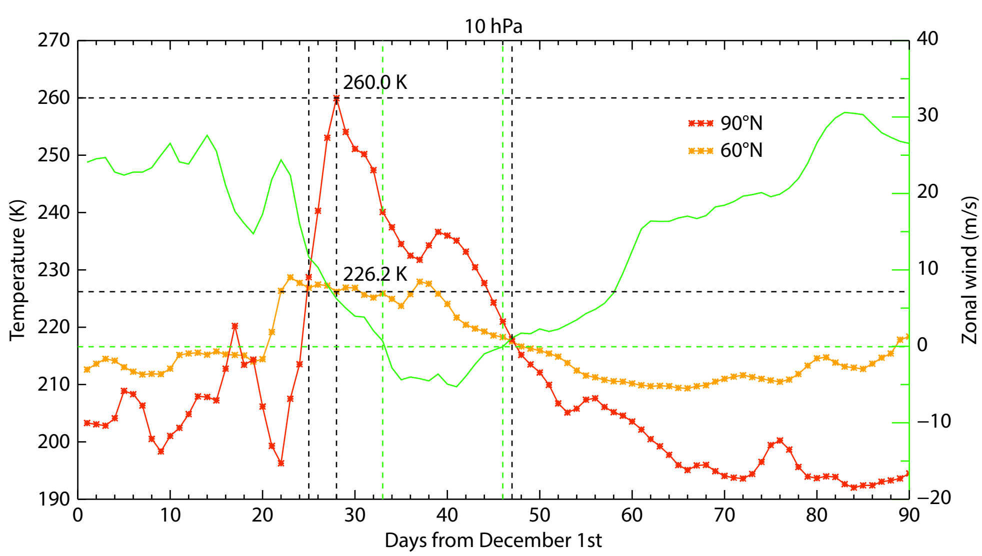

Figure 1. Winter of 2018–2019, December 1 to February 28. Daily mean temperatures at 90°N and 60°N, measured at 10 hPa heights; zonal wind at 60°N, also at 10 hPa. Black dashed vertical lines from left to right represent, respectively, the onset, outbreak, and decay of the single Sudden Stratospheric Warming (SSW) event that occurred in 2018–2019. The two black dashed horizontal lines (from top to bottom of the temperature axis, left) represent, respectively, the temperatures at 90°N and 60°N at 10 hPa on the outbreak date. The green dashed vertical lines from left to right represent, respectively, the beginning and end of zonal mean wind reversal during the 2018–2019 SSW. The green dashed horizontal line marks the position of zero wind.

where $T'(\lambda)$ is the longitudinal dependent temperature fluctuation of SPWs; A, s, and φ represent amplitude, zonal wavenumber, and initial phase for the SPW oscillation, respectively. Here, we choose s = 1 and = 2 to represent SPWs with zonal wavenumber 1 and 2, respectively; λ is the longitude. The average amplitude of the three months is taken as the amplitude of the SPW with zonal wavenumber 1 (SPW1) and the SPW with zonal wavenumber 2 (SPW2) in each year, and then their trends are calculated.

To extract the monthly amplitudes of the 16DW at each pressure level and each latitude bin, the background temperature (determined by a linear fitting within a 30-day window centered at the central day of a month) was removed. Then, the 16DW amplitude and phase with specific wavenumbers were extracted from the residual temperature fluctuation by a harmonic fitting,

$$T'(t, \lambda) = A\cos((2\pi/\sigma)t + s\lambda + \varphi), \quad (2)$$

where $T'(t, \lambda)$ is the temperature fluctuation within a 30-day window; σ is the wave period, chosen to be 16 days of 16DW; t is the universal time. Since anomalies of wavenumbers 1 and 2 contribute the most to the 16DW in midwinter, and precede SSWs of both the displacement and the split types, here we chose s = −2, −1 to denote westward propagating waves with zonal wavenumbers 2 and 1, and s = 1, 2 denote eastward propagating waves with zonal wavenumbers 1 and 2, respectively, to separately fit the 16DWs with the different zonal wavenumbers. For each winter month, all 16DWs with zonal wavenumber 1 (16DW1) amplitudes (including eastward 16DW1 and westward 16DW1) are added together as 16DW1 amplitudes for each month. The average amplitude of the three months is taken as the amplitude of 16DW1 in the year, and then the trend is calculated. Take December 2018, when the SSW occurred, as an example. We have plotted the temperature at 10 hPa and 60°N to demonstrate the fitting of SPW1 and 16DW1. For the 16-day wave, in Figure 2b, we arbitrarily selected longitude 60°E to show its temporal variation. For SPW1, it can be clearly seen in Figure 2a that SPW1 mainly presents the characteristic of zonal wave number 1 with an amplitude of approximately 22.4 K. For the fitted propagating 16-day waves with zonal wavenumber 1 (16DW1), Figure 2b shows that the amplitude of eastward 16DW1 (E1) and westward 16DW1 (W1) were 5.1 K and 5.2 K, respectively. The resultant amplitude was 5.2 K.

3. Results

3.1 Long-term Trends of the SSWs

Figure 3 presents the durations and temperature differences of all SSWs (including both major and minor warmings) in each midwinter from 1980 to 2020. An SSW's duration is the number of days in which the warming was observed; the event's temperature difference measures its strength. No SSWs were observed in 1986, 1993, 1997, 2011, and 2014. We note that both the durations and temperature differences of SSWs exhibit significant inter-annual variation, implying that SSW triggering mechanisms are likely to be complex. The duration maximum (34 days) appeared around 2002 (December 2001–February 2002); the minimum (1 day) was observed around 2000 (December 1999–February 2000). The temperature difference maximum (68.0 K) and minimum (2.1 K)

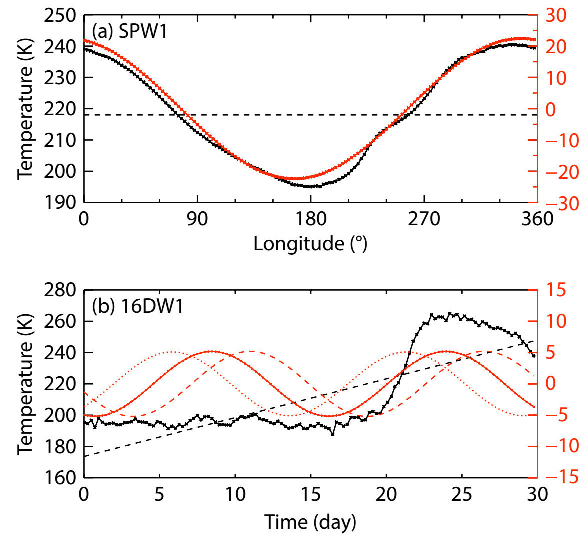

Figure 2. (a) The longitude variations of temperature at 10 hPa at 60°N in December 2018. The solid black curve, black dashed line, and red curve are the longitude-dependent monthly averaged temperature, zonal mean of the monthly averaged temperature, and fitted Stationary Planetary Wave with zonal number 1 (SPW1), respectively. (b) The time variations of temperature at 10hPa at (60°N, 60°E) from December 1, 2018, to December 31, 2018. The solid black curve and black dashed line are the raw temperature data and linear trend, respectively. Red dotted curve, red dashed curve, and red solid curve are the fitted Westward propagating 16-day waves with zonal wavenumbers 1 (W1), the fitted Eastward propagating 16-day waves with zonal wavenumbers 1 (E1), and the fitted propagating 16-Day Waves with zonal wavenumbers 1 (16DW1), respectively. The right vertical axis represents the fitted SPW1 and 16DW1 by temperature in units of K degrees.

occurred in the same years as the duration maximum and minimum — 2002 and 2000, respectively. Besides the correlation between the highest and lowest SSW durations and temperature differences, lower temperature difference peaks in 1987, 1998, 2003, and 2006 were also associated with longer SSW durations. These results indicate a high correlation (correlation coefficient of 0.74) between an SSW's duration and its zonal mean temperature difference; thus, either parameter could well and consistently characterize the SSWs and their inter-annual variations (Li YP and Wen ZP, 2021, 2022). Although there are intricate inter-annual variations over the 42 years, a small positive trend in SSW duration and strength can still be found: linear fittings, after discarding the no-SSWs years, indicate positive trends of 1.39 days per decade in SSW duration and 0.42 K per decade in temperature difference with a confidence interval of 95%, which is consistent with previous studies (Charlton-Perez et al., 2008; McLandress and Shepherd, 2009).

Although both the duration and strength of the SSWs exhibit weak increasing trends over the period 1980–2020, a previous paper by Manney et al. (2005) has argued that SSWs in the period between 1998 and 2004 had the highest SSW activity, suggesting that there may have been different trends before and after 1998–2004. Figure 3 presents compelling new evidence that remarkable winter peaks did indeed occur around the year 2002

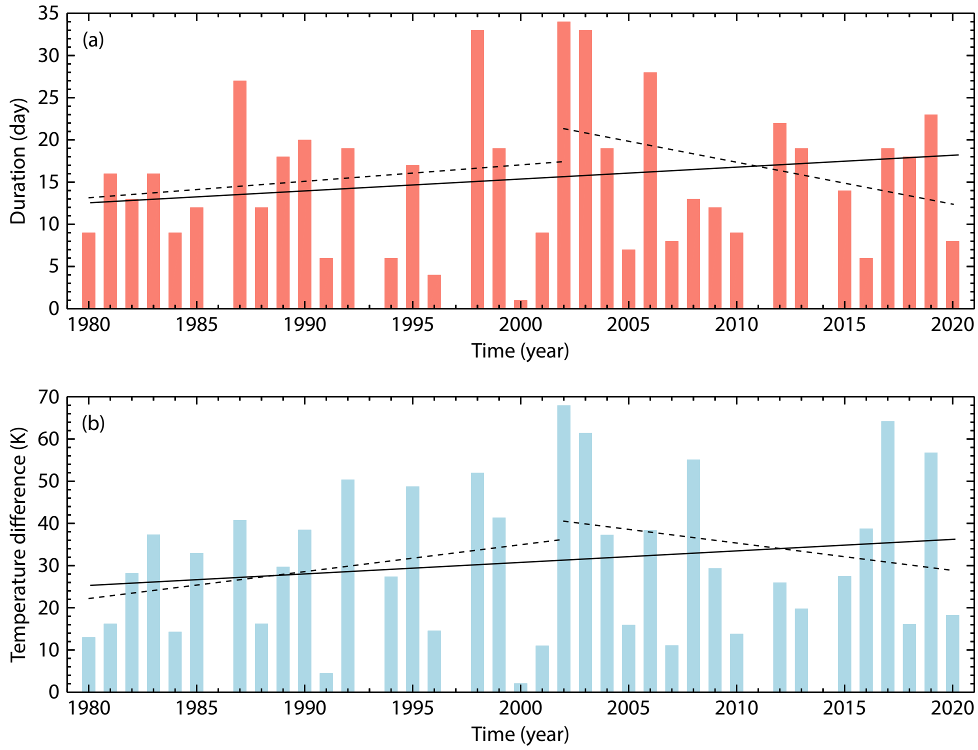

Figure 3. Duration (a) and temperature difference (b) of all SSWs in the midwinter from December 1979 to February 2020. The solid lines represent the overall linear fittings after discarding the no SSWs years; the dashed lines represent the piecewise linear fittings.

(December 2001–February 2002), which suggests that, indeed, the long-term SSW trend is not a monotonical increase with time. As mentioned above, although there are consistently increasing trends in both parameters over the 42 years, it can be observed that before 2002, both the duration and temperature difference increased, while after that, they decreased, again uniformly. Therefore, we perform piecewise linear fittings on both parameters by taking the time 2001/2002, when both parameters have maximum values, as the temporal inflection point. Here we have named the fore part to be December 1979 to February 2002; the latter part is from December 2001 to February 2020. The segmented trends are shown in Figure 3 by dashed lines. The segmented trends are, respectively, 1.9 days per decade (6.3 K per decade) before 2002 and −5.3 days per decade (−6.1 K per decade) after 2002 in duration (temperature difference). Only the temperature difference in the front segment has a confidence of 95%.

3.2 Long-term Trends of the Polar Vortices

In this section, we investigate the long-term trend of polar vortices over the same period of study. Figure 4a shows the time series of the *annual mean* PVA in the three winter months, between 60°N and 90°N, at different height ranges over the entire 41 winters from December 1979 to February 2020. Although here again there is interannual variability, it is noteworthy that the anomaly above 10 hPa varies from −200 PVU to 200 PVU with an obvious decreasing trend over the 42 years. For instance, before 2002, in all height ranges, the Potential Vorticity Anomalies (PVAs) were primarily positive; after 2002, they were primarily negative. The overall relative variations in the 42 years were −22.4%, −17.6%, −5.1%, and −4.9% in the ranges of 10–5 hPa, 10–7 hPa, 20–10 hPa, and 30–10 hPa, respectively. All the Mean Absolute Percentage Errors during 1980–2020 are less than 8%, suggesting the following link between SSW events and the polar vortices: a decreasing polar vortex trend appears to lead to an increase in SSW intensity and duration. The variation here is the result of the linear fitted trend after multiplying by time; the relative variation is then normalized — which is to say, divided by the 41-year-mean of the winter values.

An apparent trend reversal in the PVA occurred around the 2002s, opposite to the corresponding SSW trends. In Figure 4b, we present the fitted relative variation in the fore and latter time periods at different height ranges. To display the relative variation more clearly, we set the reference 2002 PVA to 0. Figure 4b clearly demonstrates that, at all concerned height ranges, the PVAs consistently exhibit negative trends in the fore part and positive trends in the latter part, opposite to the SSW trends, further confirming that the polar vortex and SSW are closely related. Moreover, it is obvious that the higher the height range, the more significant the declining (increasing) trend in the fore (latter) part. Quantitatively, the most significant relative trends in 10–5 hPa exceed (∓) 9% during 1980–2002 (2002–2020), while, in the height range of 30–10 hPa, the magnitude of the negative (positive) change drops to −6% (4%) in the fore (latter) part. All the Mean Absolute Percentage Errors during 1980–2002 (2002–2020) are less than 7% (9%). Many researchers have also reported the weakening of the stratospheric polar vortex in the recent several decades (Cohen et al., 2014; Kim et al., 2014; Zhang MH et al., 2019). Besides, Reichler et al. (2012) also revealed a correlation between variations in the weak vortex and the frequency of SSWs,

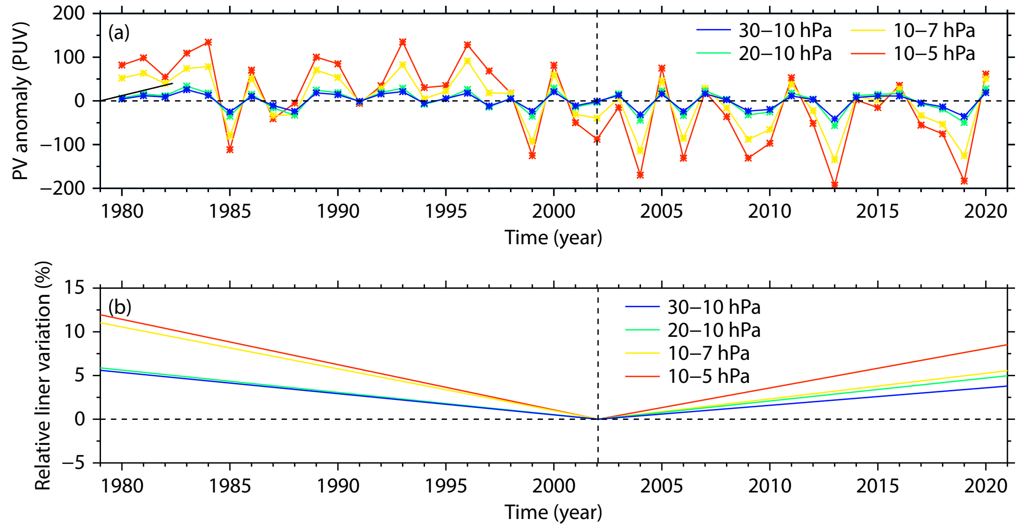

Figure 4. (a) The curves denote the monthly mean Potential Vorticity Anomalies (PVAs) from December 1979 to February 2020. (b) The piecewise linear fittings of annual winter and zonal mean PVAs averaged over 60°N–90°N at different height ranges in the fore and latter parts of the 42-year period. The purple, green, yellow, and red lines are for the relative trends at the heights of 30–10, 20–10, 10–7, and 10–5 hPa, respectively.

especially the record during the 2000s.

3.3 Long-term Trends of Planetary Waves

The other important phenomenon that appears to be involved in the triggering of SSWs is planetary waves. According to past studies (Gong Y et al., 2019; Li W et al., 2021), the waves that contribute the most to SSW triggering are the SPW and the 16DW; therefore, here in our analyses, we focus on the SPW and the 16DW only. The SPW and 16DW trends, below, were calculated by a linear fitting of the zonal mean planetary wave amplitude in the time domain at each barometric surface and latitude. Figure 5 displays the long-term trends for SPW1 in the annual winter mean temperature

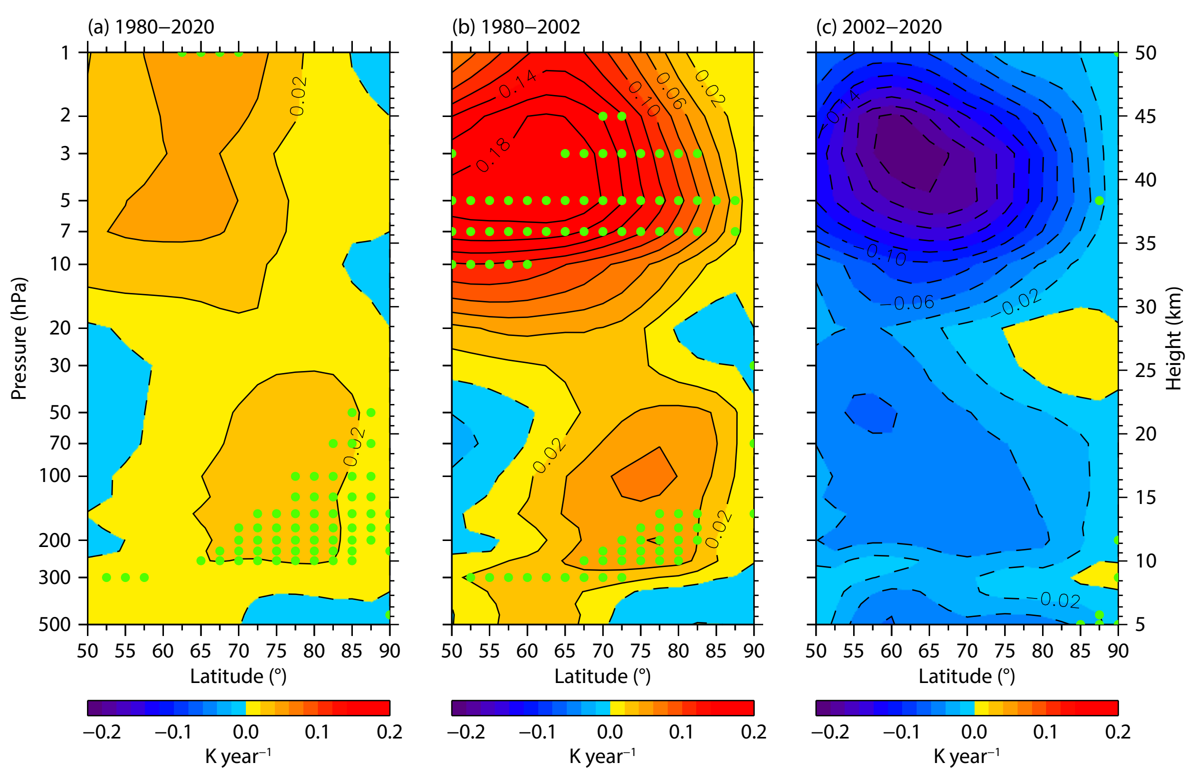

Figure 5. Latitude-pressure sections of the long-term trends (unit: K per year); contour intervals are 0.02 K per year for (a), (b), and (c) of the annual winter mean stationary planetary wave temperature amplitude with wavenumber 1 (SPW1). From (a) to (c) are the trends for 1980–2020, 1980–2002, and 2002–2020, respectively. The solid and dashed contours denote the positive and negative trends, respectively. Cyan stippling indicates results above 90% confidence level according to the two-sided Student's *t*-test.

amplitude, as a function of pressure and latitude, from a linear regression analysis over three durations, i.e., the winters of 41 years (1979/1980–2019/2020), the fore part of that time period (1979/1980–2001/2002), and the latter part (2001/2002–2019/2020). As shown in Figure 5a, SPW1 exhibits a prominent positive trend in the wide latitude range from 50°N to 90°N and in the whole pressure range from 500 to 1 hPa, with statistically significant peaks of ~0.06 K per year at ~65°N, 1 hPa. Besides, statistically significant positive areas also appear in the troposphere at latitudes higher than 65°N, suggesting a link between the SPW1 and SSWs, at least in the troposphere: the strengthening trend of the SPW1 might also be a possible factor in the SSW trends of increasing intensity and duration.

Notably, consistent with the SSWs, the SPW also exhibits a piecewise variation within the 41-winter overall increasing trend. Above 10 hPa, the SPW1 rises until 2002 and then is seen to decrease slowly. In the fore part, before 2002, the SPW1 trend is consistently positive from the troposphere to the stratosphere above most latitudes; the positive trend is statistically significant in almost the whole height range, from 50°N to 90°N, with a pronounced trend peak of 0.20 K per year at 5 hPa, around latitude 65°N. However, referring to Figure 5c (i.e., after 2002) the SPW1 trend is negative at most altitudes and latitudes, consistent with the trend of SSW parameters and contrary to the overall polar vortex trend. Although the largest negative trend does not reach 90% confidence, its maximum negative trend is as great as −0.22 K per year at 3 hPa, near 62.5°N. As to the few statistically significant negative trends observed at the edge of the Arctic polar region, around 5 hPa and below 300 hPa, the negative peaks are far weaker than the positive peak trend before 2002, confirming that the 42-year overall trend is strengthening. However, the positive trend is small and lacks sufficient statistical confidence close to the north pole below 20 hPa. Such a segmented trend, with an inflection point in the early 2002s, has also been reported by Hu DZ et al. (2019). In general, the results shown in Figure 5 further confirm the close link between the SPW1 and SSW. Apart from that, we also calculated the trend of SPW2 (not presented), finding that the SPW2 trends are rather weak and lack sufficient confidence. Therefore, we propose that, for the SPW, the main contributor to the variation in the duration and magnitude of SSWs is likely to be the SPW1.

To investigate further possible links between SSWs and the SPW, in Figure 6 we present correlation coefficients between winter mean SSW duration and SPW1 amplitudes, for the three periods mentioned above. On the whole, for all three periods, the latitudinal and height distributions of the correlation coefficients are dominated by significant positive correlations; in the troposphere, all the peak correlation coefficients exceed 0.5. Moreover, the larger positive correlation coefficient region in Figure 6 coincides with the region where the SPW1 trend is statistically significant (as shown in Figure 5). In Figure 6a, the maximum correlation coefficient reached 0.56 around 2 hPa at 57.5°N for the entire 42-year period. In the fore part, the positive correlation has more significantly positive values in a height range from 500 to 1 hPa at mid-high latitudes, with peaks of 0.71 at 2 hPa around a latitude of 55°N and 0.60 at 500 hPa around a latitude of 60°N. The maximum positive correlation coefficient can reach 0.51 located at 87.5°N at 70 hPa in the later time segment. We note that in the subperiods of 1980–2020 and 1980–2002, the correlation coefficients are statistically significant at almost all latitudes and heights. As to the period from 2002 to 2020, at least three regions meet 90% confidence: 60°N–72.5°N at 300–200 hPa, 82.5°N–87.5°N at 100–50 hPa, and 50°N to 75°N at 3–2 hPa. In short, the results shown in Figure 6 further verify a close link between the SPW1 and SSWs. In addition, we also calculated the correlations of SPW2 with SSW duration in these three periods; as expected, the correlation coefficients are rather weak and lack sufficient confidence.

To investigate whether the 16-day waves affect SSWs or not, we examine Figure 7 for the trends of 16DW1 and Figure 8 for the correlation with SSWs, where the scale measure is exactly the same as for SPW1. Similar to the SPW, Figure 7a confirms that the 16DW exhibits a significantly positive trend in most latitudinal and height regions over the entire 42-year period, consistent with the previous study by Tang WT et al. (2021). The peak trend of 0.05 K per year from December 1979 to February 2020 in 16DW1 is slightly less than that of SPW1, implying that the 16DW1 may also exert non-negligible effects on the trend of SSWs over the 42-year period. Figure 7b illustrates that in the fore part, although the positive trend is also prominent, as in the case of the SPW, there are also distinctions between the 16DW1 and SPW1 trends. For instance, the prominent positive contribution of 16DW1 is concentrated mainly at latitudes higher than 70°N and above 5 hPa in the fore part, which is apparently different from the apparent SPW1 contribution pattern. Moreover, the maximum positive trend in 16DW1 is only 0.09 K per year, far smaller than that of the SPW1 in the fore part, suggesting that, compared with the SPW1 contribution, the 16DW1 played only a minor role in SSW events in the fore part. Moreover, the 16DW1 also exhibits an obvious negative trend, with a negative peak trend of −0.03 K per year at 77.5°N at 225 hPa. With respect to the latter part in Figure 7c, the negative trend is also obvious in the 16DW1 temperature. But, distinguished from SPW1, the negative trend region occurred in the latitudes higher than 80°N and above 5 hPa, with a peak value of ~−0.09 K per year. However, there is sufficient statistically significant data here, in combination with the SPW1 trend analysis in the post-2002 years, for us to suggest that the SSW decline after 2002 may be attributable to the decreasing trend of the 16DW1. Besides, the relatively weak positive trend above, satisfying statistical confidence below 10 hPa, can also be observed, with a peak value of about 0.08 K per year. Generally, the 16DW1 trends in all three periods are consistent with those of the SPW1, suggesting non-negligible influences of 16DW1 on SSWs. Moreover, the trend (not presented) of the 16-day wave with zonal wavenumber 2 (16DW2) is also inappreciable, relative to the 16DW1, just as in the SPW.

Figure 8 displays the correlation coefficients of winter mean SSW duration and 16DW1 amplitudes over the three periods mentioned above, allowing us to examine further their linkage. Overall, similar to the SPW1 correlations, significant positive correlations are observed in all three time periods, with maximum positive values larger than 0.5. For example, the largest correlation coefficient in the latter part — larger than 0.8 — is observed at 30

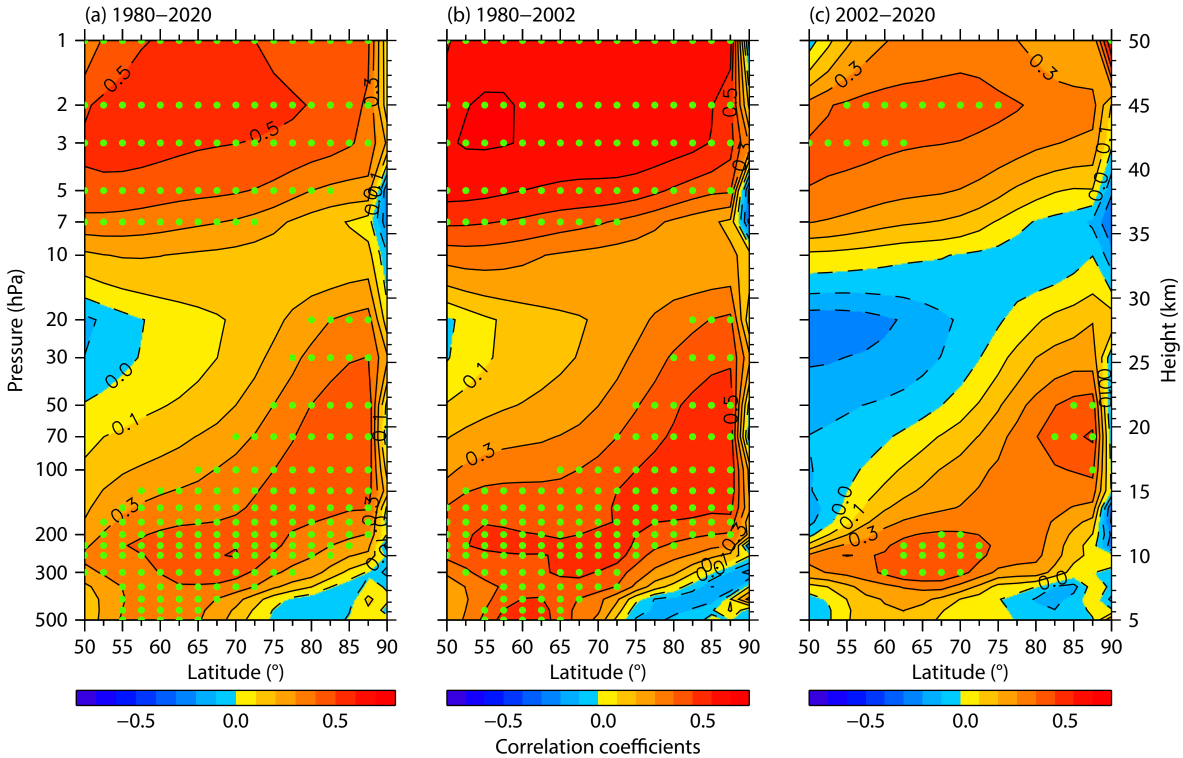

Figure 6. Latitude-pressure sections of the correlation coefficients between the winter mean duration of SSW and winter mean Stationary Planetary Wave temperature amplitude with wavenumber 1 (SPW1) (contour intervals are 0.1 for all panels). From (a) to (c) are the correlation coefficients in the periods of 1980–2020, 1980–2002, and 2002–2020, respectively. The solid and dashed contours denote positive and negative correlations, respectively. Cyan stippling indicates results above 90% confidence level according to the two-sided Student's *t*-test.

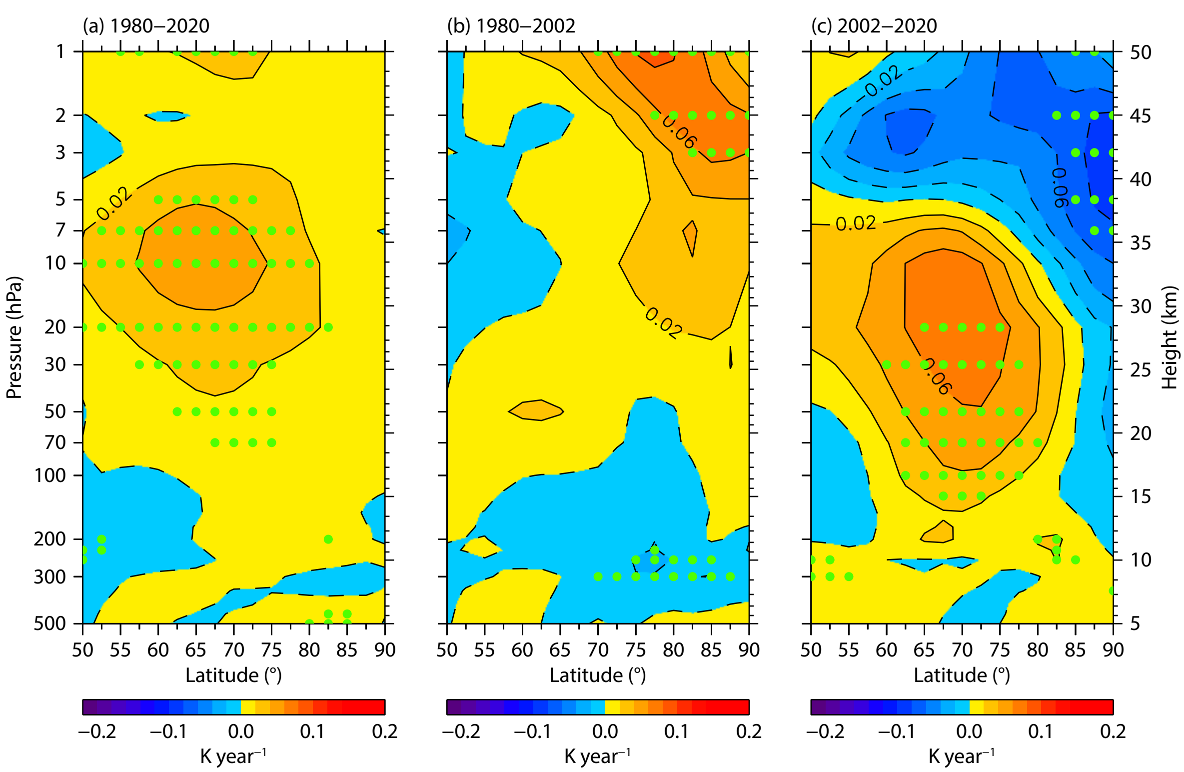

Figure 7. Latitude-pressure sections of the long-term trends (unit: K per year); contour interval is 0.02 K per year for (a), (b), and (c) of the annual winter mean 16-Day Wave with wavenumber 1 (16DW1) temperature amplitude. From (a) to (c) are the trends for 1980–2020, 1980–2002, and 2002–2020, respectively. The solid and dashed contours denote the positive and negative trends, respectively. Cyan stippling indicates results above 90% confidence level according to the two-sided Student's *t*-test.

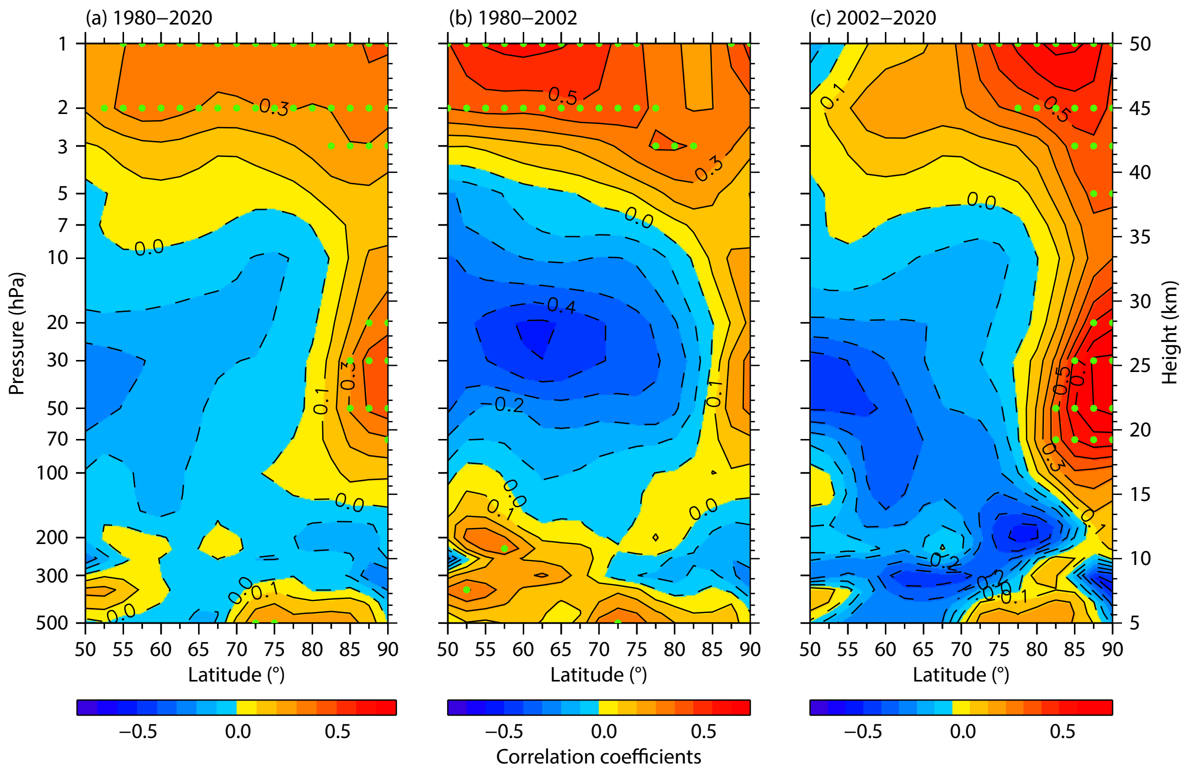

Figure 8. Latitude-pressure sections of the correlation coefficients between the winter mean duration of SSW and annual winter mean 16-Day Wave with wavenumber 1 (16DW1) (contour intervals are 0.1 for all panels). From (a) to (c) are the correlation coefficients in the periods of 1980–2020, 1980–2002, and 2002–2020, respectively. The solid and dashed contours denote the positive and negative correlations, respectively. Cyan stippling indicates results above 90% confidence level according to the two-sided Student's *t*-test.

hPa above 90°N. Most importantly, the significant positive correlations in all three periods were above 90% confidence level. These results suggest that the impact of 16DW1 on SSWs over the 41 winters (1979/1980–2019/2020) is also non-negligible, consistent with the Aura satellite study reported by Gong Y et al. (2019). There are also evident differences in the correlation coefficients between SPWs and SSWs. For instance, the positive correlation between 16DW1 and SSW is limited mainly to latitudes higher than 80°N and altitudes above 10 hPa. In other latitude and altitude ranges, the correlation is mainly negative.

4. Summary

In this paper, we utilize ERA5 data from December 1979 to February 2020 to reveal changes of SSWs in the NH and to try to identify and quantify factors that may be driving those changes. Our primary findings are summarized as follows. Over the 42 years examined here, SSWs exhibit trends of increasing duration (1.39 days per decade) and temperature gradient (0.42 K per decade), which are consistent with previous results (Li Y et al., 2023). However, our results also reveal that, within this long-term pattern, an inflection point occurred roughly in 2002: SSW durations and temperature gradients increased before 2002 but decreased after 2002, though they remained higher than in 1979. Li YP and Wen ZP (2022) also discovered that SSW duration and strength tended to increase from 1948 to 2003. After 2003, these increasing trends did not persist.

We studied polar vortices and planetary waves as possible mechanisms driving the observed long-term variations in SSW strength and duration. We found an attenuating trend in the polar vortex below 30 hPa for the whole duration of 1980–2020. Interestingly, in all different pressure ranges in 30–5 hPa, the strengths of the polar vortex in the winter became uniformly weaker until 2002 and then became stronger. The closer the height range to 5 hPa, the more significant the decreasing (increasing) trend of the polar vortex before (after) 2002. Hu DZ et al. (2018) also found that the stratospheric polar vortex strengthened during 1998–2016, contrary to its weakening trend prior to that period.

Notably, the long-term variations of SPW1s and 16DW1s correlate well with those of SSWs. Wave amplitudes of both of these PWs (with zonal wavenumber 1 components) exhibit increasing trends over the entire period from 1980 to 2020. Within that period, their amplitudes trended upward until 2002 and began to decline thereafter. However, despite their similar trends, the magnitudes of neither the SPW2 nor 16DW2 trends are substantial enough to explain the similar SSW trends over these periods. We suggest that only the trends of the PW1s satisfy sufficient statistical confidence to be likely causes of the observed SSW trends. In particular, we can assert that PW1 is likely to prove to be the primary contributor to the long-term trends of the PWs as well as the SSWs. Finally, although 16DW1 may play an important secondary role in SSW trends, the magnitude and statistical significance of SPW1 trends, correlated to SSW trends in the period of 1980–2002, suggest that SPW1 may have the most prominent effect on SSWs.

In summary, our results clearly demonstrate for the first time that, over different periods, the increasing (decreasing) trends of both the SSW duration and temperature difference are always accompanied by the decreasing (increasing) polar vortex and increasing (decreasing) planetary waves in winter. This strongly suggests that long-term variations of polar vortices and planetary waves (especially those of the SPW) significantly impact the SSWs. Consistent with previous studies, this analysis of ERA-5 data implies that the planetary wave-polar vortex interaction is remarkably successful in explaining (at least qualitatively) not only the triggering of SSWs but also the variations in the duration and magnitude of SSWs.

Acknowledgments

We are grateful to the editor and anonymous reviewers for their valuable comments on our paper. The study is supported by the National Key RandD Program of China (2022YFF0503703) and the National Natural Science Foundation of China (through grant 42127805). The authors thank the European Centre for Medium-Range Weather Forecasts (ECMWF) for the dissemination of ERA5 data. All data used in this study are publicly available.

The ERA5 reanalysis data were freely downloaded from the ECMWF Copernicus Climate Data Store (CDS); monthly products and hourly products are accessible at https://cds.climate.copernicus.eu/cdsapp#!/dataset/reanalysis-era5-pressure-levels-monthly-means?tab=form and https://cds.climate.copernicus.eu/cdsapp#!/dataset/reanalysis-era5-pressure-levels?tab=form.

References

Ambaum, M. H. P., and Hoskins, B. J. (2002). The NAO troposphere–stratosphere connection. *J. Climate*, *15*(14), 1969–1978. https://doi.org/10.1175/1520-0442(2002)015<1969:TNTSC>2.0.CO;2

Baldwin, M. P., and Holton, J. R. (1988). Climatology of the stratospheric polar vortex and planetary wave breaking. *J. Atmos. Sci.*, *45*(7), 1123–1142. https://doi.org/10.1175/1520-0469(1988)045<1123:COTSPV>2.0.CO;2

Baldwin, M. P., Ayarzagüena, B., Birner, T., Butchart, N., Butler, A. H., Charlton-Perez, A. J., Domeisen, D. I. V., Garfinkel, C. I., Garny, H., … Pedatella, N. M. (2021). Sudden stratospheric warmings. *Rev. Geophys.*, *59*(1), e2020RG000708. https://doi.org/10.1029/2020RG000708

Castanheira, J. M., and Barriopedro, D. (2010). Dynamical connection between tropospheric blockings and stratospheric polar vortex. *Geophys. Res. Lett.*, *37*(13), L13809. https://doi.org/10.1029/2010GL043819

Charlton, A. J., and Polvani, L. M. (2007). A new look at stratospheric sudden Warmings. Part I: climatology and modeling benchmarks. *J. Climate*, *20*(3), 449–469. https://doi.org/10.1175/JCLI3996.1

Charlton-Perez, A. J., Polvani, L. M., Austin, J., and Li, F. (2008). The frequency and dynamics of stratospheric sudden warmings in the 21st century. *J. Geophys. Res.: Atmos.*, *113*(D16), D16116. https://doi.org/10.1029/2007JD009571

Chau, J. L., Hoffmann, P., Pedatella, N. M., Matthias, V., and Stober, G. (2015). Upper mesospheric lunar tides over middle and high latitudes during sudden stratospheric warming events. *J. Geophys. Res.: Space Phys.*, *120*(4), 3084–3096. https://doi.org/10.1002/2015JA020998

Cohen, J., Screen, J. A., Furtado, J. C., Barlow, M., Whittleston, D., Coumou, D., Francis, J., Dethloff, K., Entekhabi, D., … Jones, J. (2014). Recent Arctic amplification and extreme mid-latitude weather. *Nat. Geosci.*, *7*(9), 627–637. https://doi.org/10.1038/ngeo2234

Coy, L., Eckermann, S., and Hoppel, K. (2009). Planetary wave breaking and tropospheric forcing as seen in the stratospheric sudden warming of 2006. *J. Atmos. Sci.*, *66*(2), 495–507. https://doi.org/10.1175/2008JAS2784.1

de la Cámara, A., Abalos, M., Hitchcock, P., Calvo, N., and Garcia, R. R. (2018). Response of Arctic ozone to sudden stratospheric warmings. *Atmos. Chem. Phys.*, *18*(22), 16499–16513. https://doi.org/10.5194/acp-18-16499-2018

Goncharenko, L. P., Coster, A. J., Plumb, R. A., and Domeisen, D. I. V. (2012). The potential role of stratospheric ozone in the stratosphere-ionosphere coupling during stratospheric warmings. *Geophys. Res. Lett.*, *39*(8), L08101. https://doi.org/10.1029/2012GL051261

Gong, Y., Ma, Z., Lv, X. D., Zhang, S. D., Zhou, Q. H., Aponte, N., and Sulzer, M. (2018). A study on the quarter diurnal tide in the thermosphere at Arecibo during the February 2016 sudden stratospheric warming event. *Geophys. Res. Lett.*, *45*(23), 13142–113149. https://doi.org/10.1029/2018GL080422

Gong, Y., Wang, H. L., Ma, Z., Zhang, S. D., Zhou, Q. H., Huang, C. M., and Huang, K. M. (2019). A statistical analysis of the propagating quasi 16-day waves at high latitudes and their response to sudden stratospheric warmings from 2005 to 2018. *J. Geophys. Res.: Atmos.*, *124*(23), 12617–12630. https://doi.org/10.1029/2019JD031482

Hersbach, H., Bell, B., Berrisford, P., Hirahara, S., Horányi, A., Muñoz-Sabater, J., Nicolas, J., Peubey, C., Radu, R., … Thépaut, J. N. (2020). The ERA5 global reanalysis. *Quart. J. Roy. Meteor. Soc.*, *146*(730), 1999–2049. https://doi.org/10.1002/qj.3803

Hu, D. Z., Guan, Z. Y., Tian, W. S., and Ren, R. C. (2018). Recent strengthening of the stratospheric Arctic vortex response to warming in the central North Pacific. *Nat. Commun.*, *9*(1), 1697. https://doi.org/10.1038/s41467-018-04138-3

Hu, D. Z., Guo, Y. P., and Guan, Z. Y. (2019). Recent weakening in the stratospheric planetary wave intensity in early winter. *Geophys. Res. Lett.*, *46*(7), 3953–3962. https://doi.org/10.1029/2019GL082113

Huang, C. M., Li, W., Zhang, S. D., Chen, G., Huang, K. M., and Gong, Y. (2021). Investigation of dominant traveling 10-day wave components using long-term MERRA-2 database. *Earth, Planets Space, 73*(1), 85. https://doi.org/10.1186/s40623-021-01410-7

Kim, B. M., Son, S. W., Min, S. K., Jeong, J. H., Kim, S. J., Zhang, X. D., Shim, T., and Yoon, J. H. (2014). Weakening of the stratospheric polar vortex by Arctic sea-ice loss. *Nat. Commun.*, *5*(1), 4646. https://doi.org/10.1038/ncomms5646

Lawrence, Z. D., G. L. Manney, K. Minschwaner, M. L. Santee, and A. Lambert (2015), Comparisons of polar processing diagnostics from 34 years of the ERA-Interim and MERRA reanalyses. *Atmos. Chem. Phys.*, *15*(7), 3873–3892. https://doi.org/10.5194/acp-15-3873-2015

Li, W., Huang, C. M., and Zhang, S. D. (2021). Global characteristics of the westward-propagating quasi-16-day wave with zonal wavenumber 1 and the connection with the 2012/2013 SSW revealed by ERA-Interim. *Earth, Planets Space, 73*(1), 113. https://doi.org/10.1186/s40623-021-01431-2

Li, Y., Kirchengast, G., Schwaerz, M., and Yuan, Y. B. (2023). Monitoring sudden stratospheric warmings under climate change since 1980 based on reanalysis data verified by radio occultation. *Atmos. Chem. Phys.*, *23*(2), 1259–1284. https://doi.org/10.5194/acp-23-1259-2023

Li, Y. P., Tian, W. S., Xie, F., Wen, Z. P., Zhang, J. K., Hu, D. Z., and Han, Y. Y. (2018). The connection between the second leading mode of the winter North Pacific sea surface temperature anomalies and stratospheric sudden warming events. *Climate Dyn.*, *51*(1), 581–595. https://doi.org/10.1007/s00382-017-3942-0

Li, Y. P., and Wen, Z. P. (2021). The Influence of interdecadal changes in boreal winter teleconnections around the 1980s on planetary waves and stratospheric sudden warmings. *J. Geophys. Res.: Atmos.*, *126*(19), e2021JD035341. https://doi.org/10.1029/2021JD035341

Li, Y. P., and Wen, Z. P. (2022). Influence of tropical convective enhancement in Pacific on the trend of stratospheric sudden warmings in Northern Hemisphere. *Climate Dyn.*, *58*(9-10), 2541–2555. https://doi.org/10.1007/s00382-021-06021-2

Li, Y. X., Chen, G., Zhang, S. D., Gong, W. L., Ma, Z., Huang, K. M., and Gong, Y. (2021). Effect of semidiurnal lunar tides modulated by quasi-2-day wave on equatorial electrojet during three sudden stratospheric warming events. *Geophys. Res. Lett.*, *48*(19), e2021GL095352. https://doi.org/10.1029/2021GL095352

Limpasuvan, V., Thompson, D. W. J., and Hartmann, D. L. (2004). The life cycle of the northern hemisphere sudden stratospheric warmings. *J. Climate*, *17*(13), 2584–2596. https://doi.org/10.1175/1520-0442(2004)017<2584:TLCOTN>2.0.CO;2

Limpasuvan, V., Orsolini, Y. J., Chandran, A., Garcia, R. R., and Smith, A. K. (2016). On the composite response of the MLT to major sudden stratospheric warming events with elevated stratopause. *J. Geophys. Res.: Atmos.*, *121*(9), 4518–4537. https://doi.org/10.1002/2015JD024401

Lin, B. D. (1982). The behavior of winter stationary planetary waves forced by topography and diabatic heating. *J. Atmos. Sci.*, *39*(6), 1206–1226. https://doi.org/10.1175/1520-0469(1982)039<1206:TBOWSP>2.0.CO;2

Liu, H. X., Miyoshi, Y., Miyahara, S., Jin, H., Fujiwara, H., and Shinagawa, H. (2014). Thermal and dynamical changes of the zonal mean state of the thermosphere during the 2009 SSW: GAIA simulations. *J. Geophys. Res.: Space Phys.*, *119*(8), 6784–6791. https://doi.org/10.1002/2014JA020222

Ma, Z., Gong, Y., Zhang, S. D., Zhou, Q. H., Huang, C. M., Huang, K. M., Yu, Y., Li, G. Z., Ning, B. Q., and Li, C. (2017). Responses of quasi 2 day waves in the MLT region to the 2013 SSW revealed by a meteor radar chain. *Geophys. Res. Lett.*, *44*(18), 9142–9150. https://doi.org/10.1002/2017GL07459

Ma, Z., Gong, Y., Zhang, S., Luo, J., Zhou, Q., Huang, C., and Huang, K. (2020). Comparison of stratospheric evolution during the major sudden stratospheric warming events in 2018 and 2019. *Earth Planet. Phys.*, *4*(5), 493–503. https://doi.org/10.26464/epp2020044

Ma, Z., Gong, Y., Zhang, S. D., Xiao, Q., Huang, C. M., and Huang, K. M. (2024). Quasi-5-day oscillations during arctic major sudden stratospheric warmings from 2005 to 2021. *J. Geophys. Res.: Space Phys.*, *129*(4), e2023JA032292. https://doi.org/10.1029/2023JA032292

Manney, G. L., Krüger, K., Sabutis, J. L., Sena, S. A., and Pawson, S. (2005). The remarkable 2003–2004 winter and other recent warm winters in the Arctic stratosphere since the late 1990s. *J. Geophys. Res.: Atmos.*, *110*(D4), D04107. https://doi.org/10.1029/2004JD005367

Manney, G. L., Harwood, R. S., MacKenzie, I. A., Minschwaner, K., Allen, D. R., Santee, M. L., Walker, K. A., Hegglin, M. I., Lambert, A., … Fuller, R. A. (2009a). Satellite observations and modeling of transport in the upper troposphere through the lower mesosphere during the 2006 major stratospheric sudden warming. *Atmos. Chem. Phys.*, *9*(14), 4775–4795. https://doi.org/10.5194/acp-9-4775-2009

Manney, G. L., Schwartz, M. J., Krüger, K., Santee, M. L., Pawson, S., Lee, J. N., Daffer, W. H., Fuller, R. A., and Livesey, N. J. (2009b). Aura microwave limb sounder observations of dynamics and transport during the record-breaking 2009 arctic stratospheric major warming. *Geophys. Res. Lett.*, *36*(12), L12815. https://doi.org/10.1029/2009GL038586

Manney, G. L., Santee, M. L., Rex, M., Livesey, N. J., Pitts, M. C., Veefkind, P., Nash, E. R., Wohltmann, I., Lehmann, R., ... Zinoviev, N. S. (2011). Unprecedented Arctic ozone loss in 2011. *Nature.*, *478*(7370), 469–475. https://doi.org/10.1038/nature10556

Martius, O., Polvani, L. M., and Davies, H. C. (2009). Blocking precursors to stratospheric sudden warming events. *Geophys. Res. Lett.*, *36*(14), L14806. https://doi.org/10.1029/2009GL038776

Matsuno, T. (1971). A dynamical model of the stratospheric sudden warming. *J. Atmos. Sci.*, *28*(8), 1479–1494. https://doi.org/10.1175/1520-0469(1971)028<1479:ADMOTS>2.0.CO;2

Matthewman, N. J., Esler, J. G., Charlton-Perez, A. J., and Polvani, L. M. (2009). A new look at stratospheric sudden warmings. Part III: polar vortex evolution and vertical structure. *J. Climate*, *22*(6), 1566–1585. https://doi.org/10.1175/2008JCLI2365.1

Matthias, V., Hoffmann, P., Rapp, M., and Baumgarten, G. (2012). Composite analysis of the temporal development of waves in the polar MLT region during stratospheric warmings. *J. Atmos. Solar Terr. Phys.*, *90-91*, 86–96. https://doi.org/10.1016/j.jastp.2012.04.004

McLandress, C., and Shepherd, T. G. (2009). Impact of climate change on stratospheric sudden warmings as simulated by the Canadian middle atmosphere model. *J. Climate*, *22*(20), 5449–5463. https://doi.org/10.1175/2009JCLI3069.1

Nash, E. R., Newman, P. A., Rosenfield, J. E., and Schoeberl, M. R. (1996). An objective determination of the polar vortex using Ertel's potential vorticity. *J. Geophys. Res.: Atmos.*, *101*(D5), 9471–9478. https://doi.org/10.1029/96JD00066

Ning, W. H., Huang, K. M., Zhang, S. D., Huang, C. M., Gong, Y., and Ma, Z. (2022). A statistical investigation of inertia gravity wave activity based on MST radar observations at Xianghe (116.9°E, 39.8°N), China. *J. Geophys. Res.: Atmos.*, *127*(1), e2021JD035315. https://doi.org/10.1029/2021JD035315

O'Neill, A., Charlton-Perez, A. J., and Polvani, L. M. (2015). MIDDLE ATMOSPHERE | stratospheric sudden warmings. In G. R. North, et al. (Eds.), *Encyclopedia of Atmospheric Sciences* (2nd ed, pp. 30-40). London: Academic Press. https://doi.org/10.1016/B978-0-12-382225-3.00230-9

Pancheva, D., Mukhtarov, P., Mitchell, N. J., Merzlyakov, E., Smith, A. K., Andonov, B., Singer, W., Hocking, W., Meek, C., … Murayama, Y. (2008). Planetary waves in coupling the stratosphere and mesosphere during the major stratospheric warming in 2003/2004. *J. Geophys. Res.: Atmos.*, *113*(D12), D12105. https://doi.org/10.1029/2007JD009011

Pedatella, N. M., Richmond, A. D., Maute, A., and Liu, H. L. (2016). Impact of semidiurnal tidal variability during SSWs on the mean state of the ionosphere and thermosphere. *J. Geophys. Res.: Space Phys.*, *121*(8), 8077–8088. https://doi.org/10.1002/2016JA022910

Pogoreltsev, A. I., Savenkova, E. N., Aniskina, O. G., Ermakova, T. S., Chen, W., and Wei, K. (2015). Interannual and intraseasonal variability of stratospheric dynamics and stratosphere–troposphere coupling during northern winter. *J. Atmos. Solar Terr. Phys.*, *136*, 187–200. https://doi.org/10.1016/j.jastp.2015.08.008

Polvani, L. M., and Waugh, D. W. (2004). Upward wave activity flux as a precursor to extreme stratospheric events and subsequent anomalous surface weather regimes. *J. Climate*, *17*(18), 3548–3554. https://doi.org/10.1175/1520-0442(2004)017<3548:UWAFAA>2.0.CO;2

Reichler, T., Kim, J., Manzini, E., and Kröger, J. (2012). A stratospheric connection to Atlantic climate variability. *Nat. Geosci.*, *5*(11), 783–787. https://doi.org/10.1038/ngeo1586

Sassi, F., Garcia, R. R., and Hoppel, K. W. (2012). Large-scale rossby normal modes during some recent northern hemisphere winters. *J. Atmos. Sci.*, *69*(3), 820–839. https://doi.org/10.1175/JAS-D-11-0103.1

Scott, R. K., and Polvani, L. M. (2006). Internal variability of the winter stratosphere. Part I: time-independent forcing. *J. Atmos. Sci.*, *63*(11), 2758–2776. https://doi.org/10.1175/JAS3797.1

Solomon, A. (2014). Wave activity events and the variability of the stratospheric polar vortex. *J. Climate*, *27*(20), 7796–7806. https://doi.org/10.1175/JCLI-D-13-00756.1

Tang, W. T., Zhang, S. D., Huang, C. M., Huang, K. M., Gong, Y., and Gan, Q. (2021). Latitudinal- and height-dependent long-term climatology of propagating quasi-16-day waves in the troposphere and stratosphere. *Earth Planets Space*, *73*(1), 210. https://doi.org/10.1186/s40623-021-01544-8

Tao, M., Konopka, P., Ploeger, F., Grooß, J. U., Müller, R., Volk, C. M., Walker, K. A., and Riese, M. (2015). Impact of the 2009 major sudden stratospheric warming on the composition of the stratosphere. *Atmos. Chem. Phys.*, *15*(15), 8695–8715. https://doi.org/10.5194/acp-15-8695-2015

Vineeth, C., Pant, T. K., Kumar, K. K., Ramkumar, G., and Sridharan, R. (2009). Signatures of low latitude–high latitude coupling in the tropical MLT region during sudden stratospheric warming. *Geophys. Res. Lett.*, *36*(20), L20104. https://doi.org/10.1029/2009GL040375

Walterscheid, R. L., Sivjee, G. G., and Roble, R. G. (2000). Mesospheric and lower thermospheric manifestations of a stratospheric warming event over Eureka, Canada (80°N). *Geophys. Res. Lett.*, *27*(18), 2897–2900. https://doi.org/10.1029/2000GL003768

Wu, D. L., Hays, P. B., and Skinner, W. R. (1995). A least squares method for spectral analysis of space-time series. *J. Atmos. Sci.*, *52*(20), 3501–3511. https://doi.org/10.1175/1520-0469(1995)052<3501:ALSMFS>2.0.CO;2

Yamazaki, Y., Matthias, V., Miyoshi, Y., Stolle, C., Siddiqui, T., Kervalishvili, G., Laštovička, J., Kozubek, M., Ward, W., … Alken, P. (2020). September 2019 Antarctic sudden stratospheric warming: quasi-6-day wave burst and ionospheric effects. *Geophys. Res. Lett.*, *47*(1), e2019GL086577. https://doi.org/10.1029/2019GL086577

Zeng, X. Y., and Zhong, G. (2024). Analysis of gravity wave activity during stratospheric sudden warmings in the northern hemisphere. *Earth Planet. Phys.*, *8*(2), 415–422. https://doi.org/10.26464/epp2024007

Zhang, M. H., Perrie, W., and Long, Z. X. (2019). Decadal variations in the winter Beaufort high and the stratospheric polar vortex. *Geophys. Res. Lett.*, *46*(9), 4933–4941. https://doi.org/10.1029/2018GL081426